Effect of Fast Acting Power Controller of Battery Energy Storage Systems in the Under-frequency Load Shedding Scheme

F. Gonzalez-Longatt
The Wolfson School: Electronic, Electrical and System Engineering
Loughborough University,
Loughborough UK
fglongatt@fglongatt.org

Jose Luis Rueda
Delft University of Technology
Department of Electrical Sustainable Energy
Delft, The Netherlands
J.L.RuedaTorres@tudelft.nl

Ernesto Vázquez Martínez
Universidad Autónoma de Nuevo León
Dept. of Electrical Engineering
Monterrey, México
evazquezmtz@gmail.com

***Abstract*—This paper presents the assessment of the effect of fast acting power (FAP) controller in the battery energy storage system (BESS) the under-frequency load shedding (UFLS) scheme. Theoretical and practical discussions about the implementation of inertia frequency control for BESS are presented in this paper. The effect of changes in the gain of the synthetic inertial on the system frequency response is investigated using time domain simulations based on DIgSILENT PowerFactory.**

***Keywords*—battery energy storage system, control system, frequency response; frequency, frequency response, inertia response.**

I. INTRODUCTION

One important challenge of future power systems is the massive deployment of power converters (PC) [1, 2]. The high PCs decouple the energy sources from the pre-existent power grids, negatively affecting the system performance [3]. During a system frequency disturbance (SFD) the balance between the power generation and demand is lost, as a consequence, the system frequency will change at a rate initially determined by the total system inertia (H_T) and the size of the power imbalance (ΔP). System inertia is proportional to the sum of *stored energy* (E_c) of the rotating masses of machines (generators and motors) which are directly connected to the electricity grid [4].

F. Gonzalez-Longatt et alia have proposed the use of inertial frequency response for utility-scale electricity energy storage systems (EESS) in [5]. The effect of installing battery energy storage system (BESS) on grid level transmission system in order to support fast inertial frequency response has been investigated in [2], [6]. This paper is a step forward in the research of inertial frequency controllers for BESS. This paper presents the effect of inertial response controller in the *battery energy storage system* (BESS) *the under-frequency load shedding* (UFLS) scheme. Theoretical and practical discussions about the implementation of inertia frequency control for BESS are presented in this paper. Initially, Section II presents the modelling aspects of the BESS, Inertial frequency response controllers and the UFLS. Section III introduces the main indicator to assess the effect of the inertial response controller of BESS on the UFLS. Section IV presents results of numerical simulation results considering sensibility analysis on the values of synthetic inertia (H_{syn}) –the gain of the inertial frequency response controller. Finally, Section V presents conclusions and a discussion about the limitation of the inertial frequency response controller implementation in BESS and its impact on the UFLS.

II. MODELLING OF BATTERY ENERGY STORAGE SYSTEM (BESS)

There are several technologies available for Electrical Energy Storage System (EESS), some of them used a classical *three-step process.* The core of the energy storage system is the *transformation* of electrical energy into some other energy form that could be reconverted into electricity [7]. In this paper, the EESS consists of a classical battery energy storage system (BESS) –see Fig 1. A very generic model of a BESS consists of two main subsystems [7, 8]: (i) a *power conversion system* (PCS) and *the battery energy system* (BES).

The *power conversion system* uses bi-directional AC/DC converter (inverter/rectifier) as the main interface between the BES and the power grid. The PCS is used to transform the DC-voltage from the BES into AC-voltage conditions required by the power grid [2]. A set of *controllers* are included in the PCS; those control loops are designed to

978-1-5386-4291-7/18/$31.00 ©2018 IEEE

enable specific functionalities interfacing the BES and the power network. The main modelling details of those subsystems are presented in the next subsections.

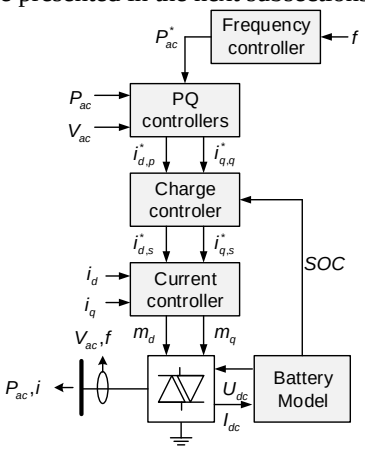

Fig. 1. A representative block diagram of a *Battery Energy Storage System* (BESS) [2].

A. Model of the Power conversion system (PCS)

This paper is focused on the system frequency response, as a consequence, the main attention is on the control behaviour of ac/dc PWM-converter instead of switching frequencies, or high frequencies phenomenon. Taking into account the previous considerations, the fundamental frequency model is used in this paper in order to model the two-level PWM converter which operated in a stator voltage oriented *dq* reference frame. *d*-axis represents the active and *q*-axis the reactive component [9].

The line-line AC voltage (rms value) is described based on *dq* reference frame as:

$$V_{ac} = V_d + jV_q \tag{1}$$

where the *d* and *q* axis component of the ac voltage are related to the dc voltage (U_{dc}):

$$V_d = \frac{\sqrt{3}}{2\sqrt{2}} m_d U_{dc} \qquad V_q = \frac{\sqrt{3}}{2\sqrt{2}} m_q U_{dc} \tag{2}$$

where m_d and m_q are the real and imaginary part of the modulation index:

$$m = m_d + jm_q \tag{3}$$

A. Model of the Battery Energy System (BES)

The BES uses reversible electrochemical reactions to convert/store electricity. There are several batteries technologies commercially available in the market [7]: *Lead-acid ba*tteries (Pb-acid), *Lithium-ion batteries* (Li-ion), *Nickel-cadmium batteries* (NiCd), *molten salt batteries* like *sodium–sulfur battery* (NaS), *aluminium-ion* (Al-ion), *vanadium redox battery* (VRB), *liquid metal batteries*, *Sodium-ion batteries* (SIB).

Batteries using Pb-acid provide a scalable technology base for providing short-term storage, in particular, frequency control. Modelling the battery is one of the most challenging situations in the energy storage system. However, since the battery is an *electric bipole*, was it linear, its more natural model would be constituted by an electromotive force (U_{in}) in series with an internal impedance (R_{in}), both function of time (t).

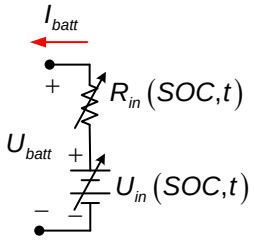

Fig. 2. Simple equivalent circuit representative of a typical electrochemical battery [2, 10].

In this paper, the simple battery model is shown in Fig. 2 is used. The *state of charge* (SOC) is calculated using an integrator which takes into account the *current of the battery* (I_{batt}):

$$U_{dc} = U_{\max} SOC + U_{\max}(1 - SOC) - I_{batt} Z_i \tag{4}$$

where U_{min} represents the cell voltage discharged cell (V), U_{max} is the maximum voltage of the battery cell (V).

B. Model of the battery charge controller

The charge controller consists of two parts (Fig. 3): (i) Charging logic to achieve the *SOC* boundary conditions ($SOC_{min} \le SOC \le SOC_{max}$), and (ii) current limiter to limits the absolute value of the current order according to limits ($I_{min} \le i \le I_{max}$). The *d*-axis current always has the higher priority than the *q*-axis current. The signal Δi is the difference between the reference *d*-axis current from the *PQ*-controller and ($i^*_{d,p}$) the modified *d*-current from the charging logic ($i^*_{d,s}$). The feedback of that signal to the *PQ*-controller prevents a windup of the PI-controller.

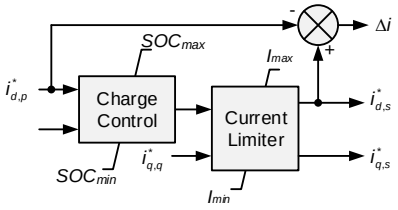

Fig. 3. Block diagram of the battery charge controller [8].

C. Model of the current controller

The input currents to the controller are the converter's AC-currents expressed in a reference *dq* frame (i_d, i_q). The output signals m_d and m_q are defined in the same reference frame and transformed back to a global reference frame using the same reference angle. A *proportional-integral* (PI) control loop is used to regulate the *d* and *q*-axis current components (i_d, i_q) based on a PI controller regulating the battery charge; these are shown in Fig. 4.

D. Model of the PQ-Controller

The controller for the active and reactive power is shown in Fig 5. The voltage (or *Q*) controller has a very slow current controller for set point tracking and a slope with a dead band

for proportional voltage support.

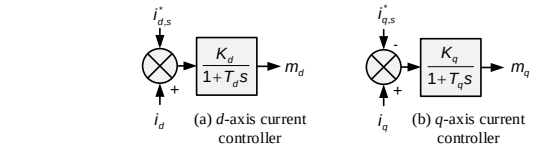

Fig. 4. Block diagram of the current controllers [2].

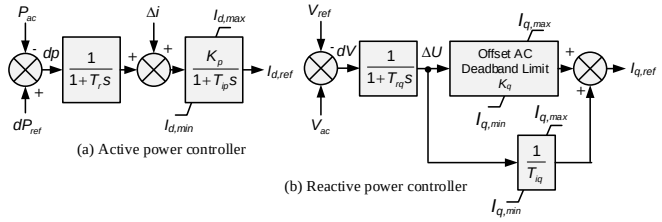

Fig. 5. Block diagram of the *PQ*-Controller.

III. Model Of Fast Active Power (FAP) Controller

This section deals with the concept of fast active power (FAP) injection/absorption as a control strategy used to enable frequency responsive mode on power electronic converter-based technologies, e.g. generation/storage. The FAP controller is mainly characterized by a very quick response, typically defined by a very short time-delay (typically related to measurement rather than activation). There is not a universal definition of FAP at the moment but delivering full power in less than a second is used in this paper. Also, this paper presents the concept of FAP controller where the core of the control action is dominated by the rate-of-change-of-the-local-frequency; there are few other controllers and proportional-limited, etc., but there are not discussed here,

Before embarking on a full discussion of the FAP control, it is important to have a clear understanding of the difference between the frequency response provided by the rotational inertial in synchronous generators and the FAP provided by power electronic converter-based technologies.

The electromechanically dynamic behaviour of a synchronous generator immediately after a system frequency disturbance is a natural consequence of the physical design of the synchronous machine. The rotor of a synchronous generator has an inherent physical characteristic called *inertia*; it quantifies the tendency of the machine rotor to resist angular acceleration. The rotational inertia is inherent of synchronous generators directly connected to the power network; it provides natural and immediately damp disturbances to system frequency.

Several controllers have been defined in the literature in order to enable the frequency response of power electronic converter-based technologies. All of those controllers actuate on the active power reference (P^*_{ac}) of the power converter by including and increment/decrement that is a function of the locally measured frequency (f). The wind turbine industry has explored and developed the concept of inertia response [11], it has several names: *Artificial, Emulated, Simulated, or Synthetic Inertia*. The inertia response concept allows a controller to the take the kinetic energy from the rotating mass in a wind turbine generator (WTG) [12]. The gain of the inertia controller (H_{syn}) has some physical meaning in the case WTG because the energy delivered to the power network is taken from the kinetic energy of rotational inertia. However, the gain of the inertia controller has not a direct interpretation in the case of non-rotating technologies, like PV, BESS, electric vehicle (EV) charger stations, etc. Some scientific papers as [7], [11] has applied the concept of inertia controller to BESS, but instead of taking kinetic energy from the rotating masses, the controller enables to discharge the battery in a controlled way producing an additional power in the form of inertial power (ΔP_{syn}).

The synthetic inertia controller can be understood as a simple loop that increases the electric power output of the PCS during the initial stages of a significant downward frequency event. The inertial power or power produced during the system frequency disturbance is calculated using the equivalent to the swing equation of a synchronous generator [3]:

$$\Delta P_{syn} = 2H_{syn}\frac{df(t)}{dt} \tag{5}$$

where H_{syn} represents the value of the synthetic inertia (sec) and f is system frequency (p.u) and ΔP_{syn} represent the so-called inertia power ($P^*_{ac} = \Delta P_{syn}$, see Fig. 1).

B. Under-Frequency Load Shedding

A significant loss of generating the plant without adequate system response can produce extreme frequency excursions outside the working range of plant [13]. The under-frequency load shedding (UFLS) strategy is designed so as to balance the demand for electricity with the supply rapidly and to avoid a rapidly cascading power system failure [14]. UFLS is a widely used last resort against large low-frequency events that may cause cascading outages and even the disconnection of parts of a system. In this paper, UFLS is set to start at 59.8 Hz, and the plan consists of six load shedding steps of unequal size with the total amount of load shed of 0.10 p.u. A delay for each load shedding step is 0.1 s.

C. Performance Assessment

Several performance indicators may be used to describe and to evaluate the frequency response. However there are three main indicators are used for the assessment of system frequency response: (i) Maximum frequency gradient ($[df/dt]_{\max}$) as observed by *ROCOF* (Rate-Of-Change-Of-Frequency) relay, (ii) Frequency nadir (f_{min}) measures the minimum post-contingency frequency and (iii) Maximum steady-state frequency deviation (f_{ss}) as observed by under frequency relays, it is defined as the absolute frequency deviation from nominal frequency (f_n). In this paper, ROCOF and f_{min} are used as the main indicator to assess the system frequency response. The inertial frequency response controller releases the active power of the BESS during a system frequency disturbance; the BESS power (P_{BESS}) has a

shape that is depicted in Fig. 6, where three H_{sys} are depicted. It is simple to see if the gain of the inertia controller the power contribution increases until the P_{BESS} reach the rated power of the power converter interface, and the inertial power contribution continues until the state-of-charge (*SOC*) of the battery reaches a minimum level, stopping the contribution at t_{cut}. The performance of the UFLS is described using two indicators, the number of load shedding steps or total load power shed ($N\Delta P_{UFLS}$) and the time where the load is shed (t_i see Fig. 6).

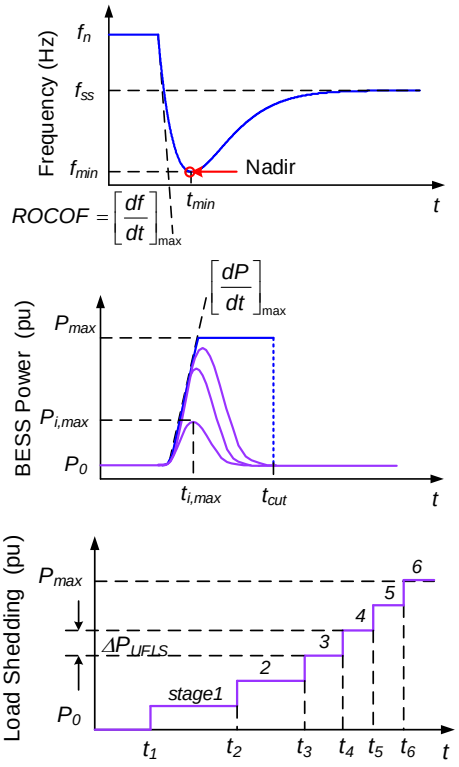

Fig. 6. Performance Indicators.

IV. Simulated Results

This section discusses the effect of inertial response controller in BESS *the under-frequency load shedding* (UFLS) scheme. Time-domain simulations using DIgSILENT PowerFactory [15] are used to assess the effects of changing H_{sys} on the inertial frequency controller of BESS. A multi-machine system is used for illustrative purposes. The test system consists of the famous WSCC 3-machine [16, 17], a 9-bus system which well-known P.M Anderson 9-bus[18]. It contains 3 generators, 6 lines, 3 loads and 3 two winding power transformers. Generators G1 is equipped with a hydro turbine governor (HYDRO) [19], and G2 and G3 use gas turbine governor (GAST) [20], and the three generators are equipped with IEEE Type 1 (1968) excitation system [21].

The total kinetic energy stored in the system at synchronous speed is 3321.90 MW·s. A system frequency disturbance is applied to the system to excite the system frequency response, it consists of the sudden disconnection of generator G2 and it creates a power imbalance ΔP = 85 MW (~27% total load). The frequency disturbance produces a quick frequency decline with a maximum *ROCOF* of -0.4709 pu/sec (~28.2 Hz/sec) and the minimum frequency of f_{min} = 55.68 Hz is reached at t_{min} = 4.62 sec.

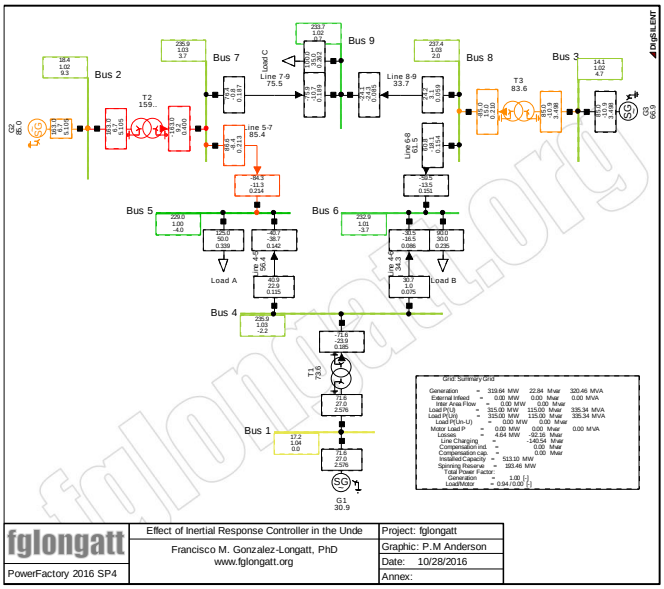

Fig. 7. *Test System*: WSCC 3-machine test system [16, 17]. Total load ΣP_L = 315 MW.

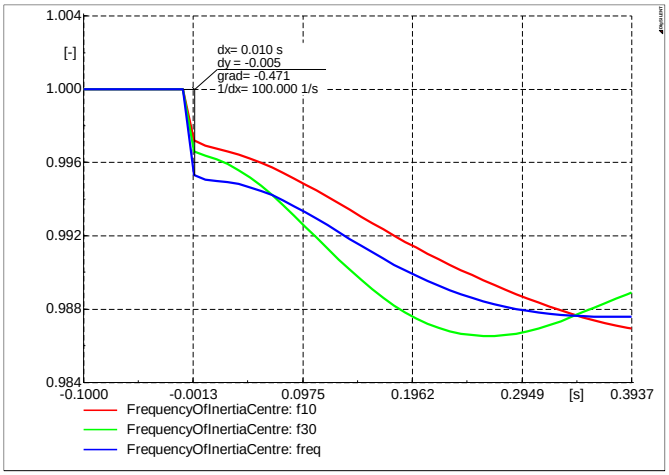

Fig. 8. System frequency response: Sudden disconnection of G2. Without-BESS and Without-UFLS.

Initially, the system frequency response of the test system is evaluated considering a considering the sudden disconnection of G2 as the system frequency disturbance. Fig 8 shows the frequency of G1 and G3 and the frequency of centre of inertia (f_{COI}) immediately after the sudden disconnection of G2, the ROCOF is also indicated.

A six-stages UFLS relay is installed on Load C (P_{load} = 100 MW, see Fig. 7), the main setting of the under-frequency relay is shown in Table I. Fig 9 shows the system frequency response and the load shed during the sudden disconnection of the generator G2. The improvement in the frequency response caused by the UFLS is clear. Although the *ROCOF* the same -0.4709 pu/sec (~28.2 Hz/sec), the minimum

978-1-5386-4291-7/18/$31.00 ©2018 IEEE

frequency is improved f_{min} = 0.953 pu (57.18 Hz) and the time 3.27 sec. Numerical results of the UFLS action are shown in Fig. 9.

TABLE I. MAIN SETTINGS OF THE UFLS RELAY

Stage	*Frequency (Hz)*	*Time (s)*	*Load Shedding (%)*
1	59.8	0.1	10.0
2	59.6	0.3	10.0
3	59.4	0.4	10.0
4	59.0	0.5	10.0
5	58.5	1.0	10.0
6	58.0	1.5	10.0

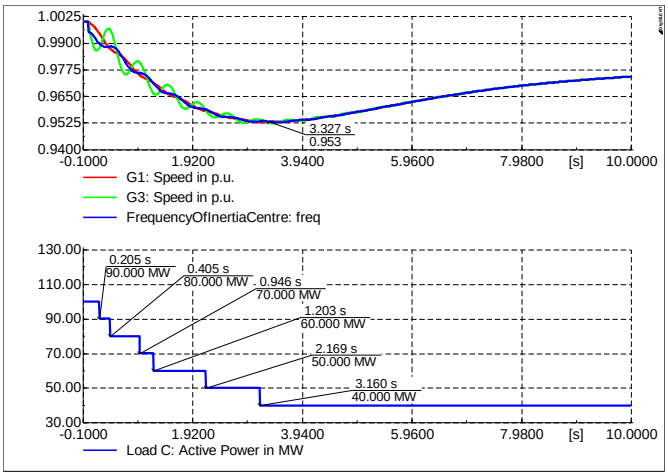

Fig. 9. System frequency response: Sudden disconnection of G2. No-BESS and With-UFLS.

Now, the BESS is connected to the test system, and FAP controller based on inertial frequency response is enabled. Sensibility analysis is performed varying the gain of the inertia controller (H_{sys}) from 0 until 200. Increasing the value of H_{sys} has a small effect on the f_{min}. Fig. 10 shows the changes on $0 \leq H_{sys} \leq 200$ produced an increase of the f_{min} between 1.0 to 22.0%. Also Fig. 10 shows the large values of H_{sys} allow a longer inertial power contribution is helping to the system frequency support (see Fig. 11) and delaying the t_{min}.

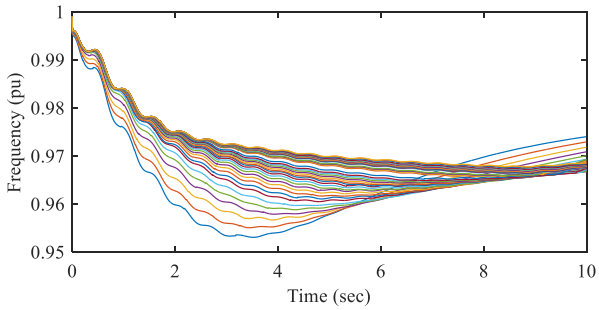

Fig. 10. System frequency response –frequency of centre of inertia, f_{COI}: Sudden disconnection of G2. With-BESS and Without-UFLS. $H_{sys} \in [0,200]$.

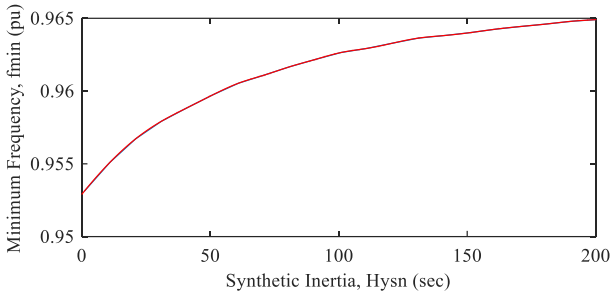

Fig. 11. The minimum frequency of inertia centre, f_{min}: Sudden disconnection of G2. With-BESS and With-UFLS.

The effect of changing the gain of the inertia controller (H_{sys}) on the time (t_{min}) when the frequency of centre of inertia reach the minimum ($f_{COI,min}$) is illustrated in Fig 12. The figure shows the clear effect of the UFLS stages, t_{min} is changing in discrete steps following the stages tripped by the UFLS. As expected, low values of H_{sys} make the fCOI to reach its minimum faster than high H_{syn}. Fig. 13 shows the acting time, the time when one stage of the UFLS is tripped. High values of H_{syn} tends to delay the acting time of each stage.

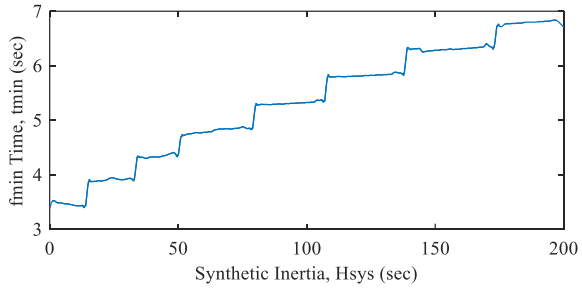

Fig. 12. Time of Minimum frequency of inertia centre, t_{min}: Sudden disconnection of G2. With-BESS and With-UFLS.

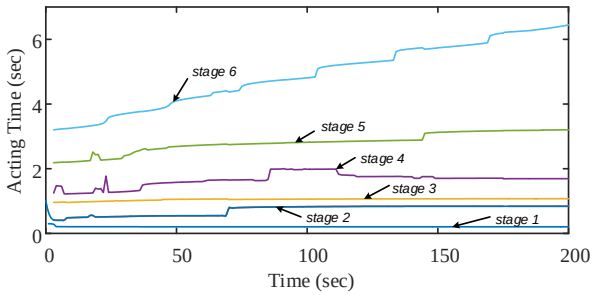

Fig. 13. Acting time of the UFLS, t_i: Sudden disconnection of G2. With-BESS and With-UFLS.

V. IV. CONCLUSIONS

This paper presents a preliminary assessment of the effect of fast acting power (FAP) controller in the battery energy storage system (BESS) the under-frequency load shedding (UFLS) scheme. Theoretical and practical discussions about the implementation of inertia frequency control for BESS are presented in this paper. The effect of changes in the gain of the synthetic inertial on the system frequency response is investigated using time domain simulations based on DIgSILENT® PowerFactory™. The FAP controller with a high value of the gain of the inertia controller helps to delay the UFLS action.

978-1-5386-4291-7/18/$31.00 ©2018 IEEE

VI. Appendix

TABLE A. Battery Models parameters

Description	*Parameter*	*Unit*	*Value*
State of change	*SOC*	-	0.8
Single Cell Capacity	W_n	Ah	1.2
Min. Voltage of an empty cell	U_{min}	V	12.00
max. Voltage of full cell	U_{max}	V	13.85
Number of parallel connected cells	N_p	-	60
Number of parallel connected cells	N_s	-	65
Nominal BESS Voltage	U_n	V	900
Internal Resistance per cell	Z_i	Ω	0.001

TABLE B. Battery Charger controller parameters

Description	*Parameter*	*Unit*	*Value*
Min charge current	*Imin*	*p.u.*	0.1
Min state of charge	SOC_{min}	*p.u.*	0.0
Max state of charge	SOC_{max}	*p.u.*	1.0
Max absolute current	I_{max}	*p.u*	1.0

TABLE C. Current controller parameters

Description	*Parameter*	*Unit*	*Value*
Proportional gain, *d*-axis	K_d	-	0.1
Integration time constant, *d*-axis	T_d	*sec*	0.001
Proportional gain, *q*-axis	K_q	-	0.1
Integration time constant, *q*-axis	T_q	*sec*	0.001

TABLE D. Current controller parameters

Description	*Parameter*	*Unit*	*Value*
Filter time constant, *d*-axis	T_r	*sec*	0.05
Filter time contact, *q*-axis	T_{rq}	*sec*	0.01
Proportional gain, *d*-axis	K_p	-	2.00
Integration time constant, *d*-axis	T_d	*sec*	0.10
Deadband for proportional gain	K_{db}	-	0.10
Proportional gain, *q*-axis	K_q	-	2.00
Integrator time constant, *q*-axis	T_q	*sec*	1.00
Min. current, *d*-axis	I_{dmin}	*p.u.*	-1.00
Min. current, *q*-axis	I_{qmin}	*p.u.*	1.00
Max. current, *d*-axis	I_{dmax}	*p.u.*	-1.00
Min. current, *q*-axis	I_{qmax}	*p.u.*	1.00

VII. References

[1] A. Bonfiglio, F. Gonzalez-Longatt, and R. Procopio, "Integrated Inertial and Droop Frequency Controller for Variable Speed Wind Generators," *WSEAS Transactions on Environment and Development*, vol. 12, no. 18, pp. 167-177, 2016.

[2] S. Alhejaj and F. Gonzalez-Longatt, "Investigation on grid-scale BESS providing Inertial Response Support," presented at the IEEE PES POWERCON 2016, Wollongong Australia, 28 September – 1 October 2016, 2016.

[3] F. Gonzalez-Longatt, "Frequency Control and Inertial Response Schemes for the Future Power Networks," in *Large Scale Renewable Power Generation*, J. Hossain and A. Mahmud, Eds. (Green Energy and Technology: Springer Singapore, 2014, pp. 193-231.

[4] A. A. Bonfiglio, F. Gonzalez-Longatt, and R. Procopio, "Evaluation of Inertial Frequency Support Provided by Variable Speed Wind Generators," presented at the 10th International Conference on Renewable Energy Sources (RES '16), Prague, Czech Republic, 18-20 March 2016, 2016.

[5] F. Gonzalez-Longatt; and S. Alhejaj, "Enabling Inertial Response in Utility-Scale Battery Energy Storage System," presented at the IEEE PES Innovative Smart Grid Technologies 2016 Asian Conference (ISGT Asia 2016), Melbourne, Australia, Nov 28 - Dec 1, 2016, 2016.

[6] S. Alhejaj and F. Gonzalez-Longatt, "Grid-Scale BESS with Inertial Response Support," presented at the International Conference for Students on Applied Engineering, ICSAE 2016, Newcastle Upon Tyne, UK, 20-21 October, 2016, 2016.

[7] F. M. Gonzalez-Longatt and S. M. Alhejaj, "Enabling inertial response in utility-scale battery energy storage system," in *2016 IEEE Innovative Smart Grid Technologies - Asia (ISGT-Asia)*, 2016, pp. 605-610.

[8] S. M. Alhejaj and F. M. Gonzalez-Longatt, "Impact of inertia emulation control of grid-scale BESS on power system frequency response," in *2016 International Conference for Students on Applied Engineering (ICSAE)*, 2016, pp. 254-258.

[9] M. Deepak, R. J. Abraham, F. M. Gonzalez-Longatt, D. M. Greenwood, and H.-S. Rajamani, "A novel approach to frequency support in a wind integrated power system," *Renewable Energy*, vol. 108, pp. 194-206, 8// 2017.

[10] M. Ceraolo, "New dynamical models of lead-acid batteries," *IEEE Transactions on Power Systems*, vol. 15, no. 4, pp. 1184-1190, 2000.

[11] F. Gonzalez-Longatt, "Impact of emulated inertia from wind power on under-frequency protection schemes of future power systems," (in English), *Journal of Modern Power Systems and Clean Energy*, pp. 1-8, 2015/08/12 2015.

[12] A. Bonfiglio, F. Delfino, F. Gonzalez-Longatt, and R. Procopio, "Steady-state assessments of PMSGs in wind generating units," *International Journal of Electrical Power & Energy Systems*, vol. 90, pp. 87-93, 9// 2017.

[13] H. Bevrani, *Robust power system frequency control : robust techniques*, 1st ed. (Power electronics and power systems). New York: Springer, 2009.

[14] "IEEE Guide for Abnormal Frequency Protection for Power Generating Plants," *IEEE Std C37.106-2003 (Revision of ANSI/IEEE C37.106-1987)*, pp. 0_1-34, 2004.

[15] DIgSILENT, "DIgSILENT PowerFactory 2016 SP4," 14.0.524.2 ed. Gomaringen, Germany, 2016.

[16] M. A. Pai, *Power system stability : analysis by the direct method of Lyapunov*. Amsterdam ; Oxford: Excerpta Medica, 1981.

[17] P. W. Sauer and M. A. Pai, *Power system dynamics and stability*. Upper Saddle River, NJ: Prentice Hall, 1998.

[18] P. M. Anderson and A. A. Fouad, *Power system control and stability*, Second ed. (IEEE Press Powwer Engineering Series). United States: Jhon Wiley and Sons, 2003, p. 658.

[19] "Hydraulic turbine and turbine control models for system dynamic studies," *IEEE Transactions on Power Systems*, vol. 7, no. 1, pp. 167-179, 1992.

[20] I. C. Report, "Dynamic Models for Steam and Hydro Turbines in Power System Studies," *IEEE Transactions on Power Apparatus and Systems*, vol. PAS-92, no. 6, pp. 1904-1915, 1973.

[21] "IEEE Recommended Practice for Excitation System Models for Power System Stability Studies," *IEEE Std 421.5-2016 (Revision of IEEE Std 421.5-2005)*, pp. 1-207, 2016.

978-1-5386-4291-7/18/$31.00 ©2018 IEEE